Nanofiber-Based Bulk-Heterojunction Organic Solar Cells Using Coaxial Electrospinning

Nicholas M. Bedford, Matthew B. Dickerson, Lawrence F. Drummy, Hilmar Koerner, Kristi M. Singh, Milana C. Vasudev, Michael F. Durstock, Rajesh R. Naik, and Andrew J. Steckl**

Nanofibers consisting of the bulk heterojunction organic photovoltaic (BHJ–OPV) electron donor–electron acceptor pair poly(3-hexylthiophene):phenyl-C_{61}-butyric acid methyl ester (P3HT:PCBM) are produced through a coaxial electrospinning process. While P3HT:PCBM blends are not directly electrospinnable, P3HT:PCBM-containing fibers are produced in a coaxial fashion by utilizing polycaprolactone (PCL) as an electrospinnable sheath material. Pure P3HT:PCBM fibers are easily obtained after electrospinning by selectively removing the PCL sheath with cyclopentanone (average diameter 120 ± 30 nm). These fibers are then incorporated into the active layer of a BHJ–OPV device, which results in improved short-circuit current densities, fill factors, and power-conversion efficiencies (PCE) as compared to thin-film devices of identical chemical composition. The best-performing fiber-based devices exhibit a PCE of 4.0%, while the best thin-film devices have a PCE of 3.2%. This increase in device performance is attributed to the increased in-plane alignment of P3HT polymer chains on the nanoscale, caused by the electrospun fibers, which leads to increased optical absorption and subsequent exciton generation. This methodology for improving device performance of BHJ–OPVs could also be implemented for other electron donor–electron acceptor systems, as nanofiber formation is largely independent of the PV material.

1. Introduction

Bulk heterojunction organic photovoltaic (BHJ–OPV) devices have been the topic of ever increasing research efforts due to their potential to result in printable, inexpensive solar cells which can be processed onto flexible substrates.[1–3] Typically, the active layer of the BHJ consists of an interpenetrating network of electron-donating conjugated polymers and electron-accepting fullerenes. One of the most studied BHJ–OPV systems consists of a mixture of poly(3-hexylthiophene) (P3HT) and [6,6]-phenyl-C_{61}-butyric acid methyl ester (PCBM).[1,4] It is widely accepted that for BHJ–OPV devices to be economically viable, power-conversion efficiencies (PCEs) need to reach 10%.[3,5] The highest PCE values obtained for P3HT:PCBM devices have been in the 4–5% range,[6–8] lower than the value needed to become competitive with silicon-based solar cells for commercial applications.

In order to increase the PCEs of BHJ–OPV devices, many different routes are currently being explored. One option is to use a different material system wherein the donor–acceptor pair exhibits improved transport properties, absorbs a larger portion of the solar spectrum, and/or has a bandgap arrangement which improves device efficiency compared to the P3HT:PCBM system.[9–16] Another route is to use a tandem cell architecture, in which two different and separate active layers absorb different portions of the solar spectrum.[17–20] Fine-tuning the morphology of the BHJ is also important. A high-efficiency device requires a balance between a high interfacial area of donor and acceptor moieties while maintaining large enough domain sizes for charge transport to the appropriate electrodes with minimum charge recombination. Typically, this is accomplished by thermal annealing[6,21–23] or solvent annealing.[7,24–26] More recently, other techniques, such as the use of processing additives and preformed nanofibers, have been developed to control the electron donor–electron acceptor morphology and molecular ordering.[3] Processing additives are used to more strongly solubilize one component of the mixture and generally have a higher boiling point than the bulk solvent, resulting in

N. M. Bedford, Prof. A. J. Steckl
Nanoelectronics Laboratory
Department of Electrical and Computer Engineering
University of Cincinnati
Cincinnati, OH 45221, USA
E-mail: a.steckl@uc.edu

N. M. Bedford
Department of Chemical and Materials Engineering
University of Cincinnati
Cincinnati, OH, 45221, USA

M. B. Dickerson, L. F. Drummy, H. Koerner, K. M. Singh, M. C. Vasudev, M. F. Durstock, R. R. Naik
Materials and Manufacturing Directorate
Air Force Research Laboratory
Wright Patterson Air Force Base
OH, 45433, USA
E-mail: rajesh.naik@wpafb.af.mil

DOI: 10.1002/aenm.201100674

Report Documentation Page

Form Approved
OMB No. 0704-0188

1. REPORT DATE	2. REPORT TYPE	3. DATES COVERED
2012		**00-00-2012 to 00-00-2012**

4. TITLE AND SUBTITLE	5a. CONTRACT NUMBER
Nanofiber-Based Bulk-Heterojunction Organic Solar Cells Using Coaxial Electrospinning	5b. GRANT NUMBER
	5c. PROGRAM ELEMENT NUMBER
6. AUTHOR(S)	5d. PROJECT NUMBER
	5e. TASK NUMBER
	5f. WORK UNIT NUMBER
7. PERFORMING ORGANIZATION NAME(S) AND ADDRESS(ES) **University of Cincinnati,Nanoelectronics Laboratory,Department of Electrical and Computer Engineering,Cincinnati,OH,45221**	8. PERFORMING ORGANIZATION REPORT NUMBER
9. SPONSORING/MONITORING AGENCY NAME(S) AND ADDRESS(ES)	10. SPONSOR/MONITOR'S ACRONYM(S)
	11. SPONSOR/MONITOR'S REPORT NUMBER(S)

12. DISTRIBUTION/AVAILABILITY STATEMENT
Approved for public release; distribution unlimited

13. SUPPLEMENTARY NOTES

14. ABSTRACT

Nanofi bers consisting of the bulk heterojunction organic photovoltaic (BHJ? OPV) electron donor?electron acceptor pair poly(3-hexylthiophene):phenyl- C 61 -butyric acid methyl ester (P3HT:PCBM) are produced through a coaxial electrospinning process. While P3HT:PCBM blends are not directly electrospinnable P3HT:PCBM-containing fi bers are produced in a coaxial fashion by utilizing polycaprolactone (PCL) as an electrospinnable sheath material. Pure P3HT:PCBM fi bers are easily obtained after electrospinning by selectively removing the PCL sheath with cyclopentanone (average diameter 120 ? 30 nm). These fi bers are then incorporated into the active layer of a BHJ?OPV device, which results in improved short-circuit current densities, fi ll factors and power-conversion effi ciencies (PCE) as compared to thin-fi lm devices of identical chemical composition. The best-performing fi ber-based devices exhibit a PCE of 4.0%, while the best thin-fi lm devices have a PCE of 3.2%. This increase in device performance is attributed to the increased in-plane alignment of P3HT polymer chains on the nanoscale, caused by the electrospun fi bers, which leads to increased optical absorption and subsequent exciton generation. This methodology for improving device performance of BHJ?OPVs could also be implemented for other electron donor?electron acceptor systems, as nanofi ber formation is largely independent of the PV material.

15. SUBJECT TERMS

16. SECURITY CLASSIFICATION OF:			17. LIMITATION OF ABSTRACT	18. NUMBER OF PAGES	19a. NAME OF RESPONSIBLE PERSON
a. REPORT	b. ABSTRACT	c. THIS PAGE			
unclassified	**unclassified**	**unclassified**	**Same as Report (SAR)**	**13**	

increased phase separation and thus improved device performance.[27–31] Preformed polymer nanofibers, made by using thermally driven solution-processing techniques, have been shown to have increased crystallinity, increased hole mobility, and absorption at longer wavelengths compared to films made via spin coating.[32–35] The inclusion of preformed nanofibers into the active layer of the BHJ increases device efficiency and can be used to better control active layer morphology, and is thus an attractive methodology for improving BHJ–OPV devices.

Electrospinning is a well-established and straightforward technique to create polymer fibers from a wide variety of materials with diameters ranging from tens of nanometers to several micrometers.[36–38] This continuous process allows the production of an entangled, 3D, nonwoven fiber network exhibiting a high density of fully interconnected pores throughout the material, which yields a very high-surface-area-to-volume ratio. This, coupled with the abilities to generate fibers from a large variety of materials, control fiber morphology, and create multicomponent fibers with relative ease have contributed to the recent increase in the application of electrospinning over solution-processing techniques for creating nanofibers. High-throughput, industrial-scale electrospinning is now achievable,[39–43] further extending the use of electrospun fibers in real-world applications. Application areas for electrospinning are varied and include biomedicine,[44,45] photonics,[46,47] catalysis,[48,49] energy storage,[50,51] energy harvesting,[52,53] and filtration.[54,55]

In this study, the use and incorporation of preformed P3HT:PCBM nanofibers produced by coaxial electrospinning[56,57] is examined for BHJ–OPV devices. Previously, P3HT fibers have been made using various electrospinning techniques for field-effect transistor,[58–60] sensor,[61] and nanoelectronic[62,63] applications. However, these methods are inappropriate for implementation in the production of OPVs. To obtain fibers, the P3HT either needs to be mixed with a high molecular weight coil-like insulating polymer that can be electrospun into uniform fibers, or to be electrospun at fairly high concentrations. The resulting fibers are often too large to be useful in OPV devices (>1 μm). Furthermore, adding PCBM to these optimized electrospinning protocols leads to poor fiber formation (based on our observations). The inability to form nanofibers from solutions of P3HT:PCBM can be attributed to the high miscibility of PCBM into P3HT,[64,65] which would perturb the P3HT chain entanglements required for fiber formation. Recently, Sundarrajan et al.[66] used coaxial electrospinning to entrap a core phase of P3HT:PCBM in poly(vinyl pyrrolidone) (PVP). After the removal of PVP, micrometer-sized fibers of P3HT:PCBM were obtained. While a novel process, the resulting nonwoven matrix of P3HT:PCBM fibers yielded a power-conversion efficiency (PCE) of 8.7×10^{-8}, a value significantly lower than that needed to be useful in PV applications. In the current study, poly(caprolactone) (PCL) is used as the sacrificial sheath and the driving force for fiber formation. P3HT:PCBM fibers are obtained by inserting a relatively dilute solution of P3HT:PCBM into the core of a charged PCL liquid jet via a concentric nozzle. The coaxial fibers are then selectively stripped of the PCL sheath, yielding pure P3HT:PCBM fibers. The resulting structurally ordered fibers of P3HT:PCBM are then incorporated into a typical active layer of a BHJ–OPV by depositing a fully solubilized P3HT:PCBM layer on top. While partial dissolution of the fibers does occur, the remaining electrospun material maintains structural coherence and acts as a template for the fully solubilized P3HT. As the mechanism of electrospun fiber formation is largely independent of the core solution, this method can be used to create nanofibers from other electron donor–electron acceptor pairs and lead to improved device characteristics for those systems.

2. Results and Discussion

Coaxial electrospinning was used to create P3HT:PCBM–PCL core–sheath fibers, which were subsequently stripped of the PCL sheath layer and embedded within the active layer of a BHJ–OPV. This was accomplished by first depositing a layer of P3HT:PCBM fibers onto the ITO:PEDOT electrode followed by depositing a backfill layer of fully solublized P3HT:PCBM. This was done to interconnect the fibers and to prevent the two electrodes from coming into contact due to the porous nature of the deposited fibers (see Experimental Section for details). The process is shown schematically in **Figure 1**. The overall fiber morphology of the as-made coaxial fibers is shown in Figure 1a. As seen in the transmission electron microscope (TEM) micrograph in Figure 1b, a uniform core–sheath structure was obtained between the PCL sheath phase and P3HT:PCBM core phase, with fiber diameters as large as 1.5 μm and as low as 300 nm. The average outer fiber diameter was 650 ± 500 nm (Figure 1a). Such a size distribution is not uncommon for electrospun fibers.[67–69] P3HT:PCBM fibers ware obtained by dissolving the PCL sheath in cyclopentanone, a solvent which does not dissolve P3HT or PCBM. The resulting P3HT:PCBM fibers are shown in Figure 1c,d. The high-resolution TEM micrograph in Figure 1d shows short-range P3HT chain stacking (~10 nm in length), despite the absence of thermal annealing. It has been previously reported[36,70–72] that molecular stacking and ordering along the fiber direction occurs in electrospun fibers due to the intense shear forces encountered in the polymer solution during electrospinning. The P3HT:PCBM fibers had diameters of 120 ± 30 nm, but tended to arrange into 500 ± 100 nm-wide fiber-like structures (Figure 1c). The P3HT:PCBM fibers were approximately on the size scale of active layer film thicknesses utilized in efficient OPV devices. If instead of using the coaxial approach described above, homogeneous solutions of P3HT, PCBM, and PCL (or poly(ethylene oxide); PEO) were electrospun, then nanofibers were not obtained after removal of the PCL or PEO. Instead, the removal of the insulating polymer phase resulted in either micrometer-sized spherical aggregates or similar-sized fibers (Figure S1, Supporting Information), neither of which would be beneficial for BHJs as charge recombination dominates in thicker films.[73,74] However, it has been observed[59] that electrospinning a solution of only P3HT and PCL yields nanoscale P3HT fibers after stripping away the PCL, indicating that the addition of PCBM greatly influences the phase separation between the two polymers within the blended electrospun fibers. This highlights the advantage of coaxial electrospinning, as the separation between PV and insulating materials is better controlled and the electrospinning process is largely controlled by the properties of the sheath solution.[75]

DOI: 10.1002/aenm.201100674

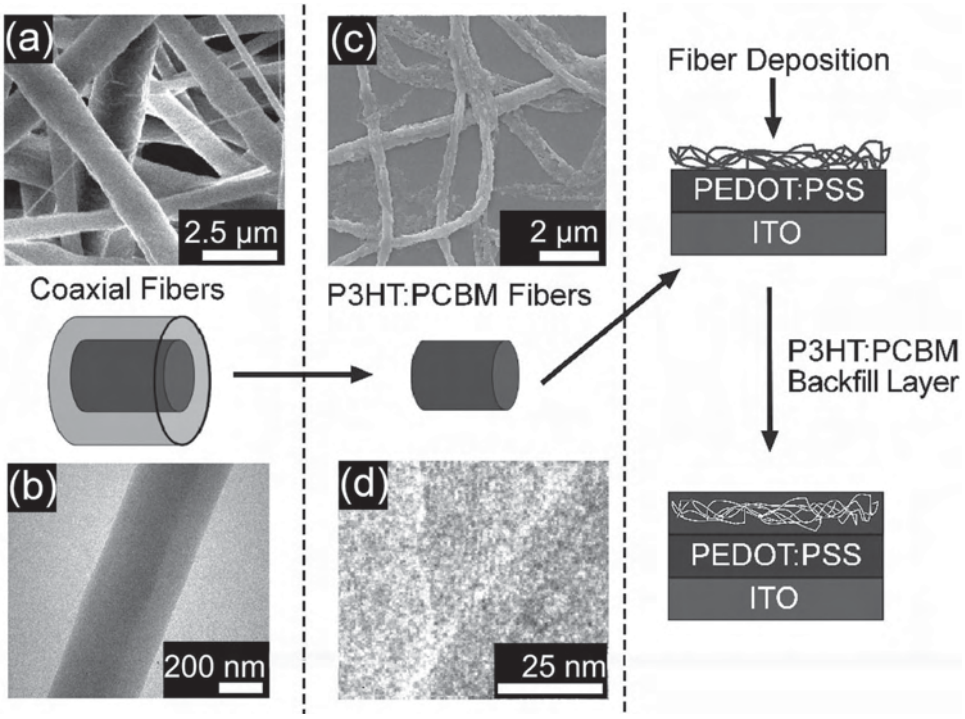

Figure 1. A schematic depicting P3HT:PCBM fiber generation from the coaxial fibers and the subsequent deposition of nanofibers within the active layer of the BHJ–OPV device, along with a) a scanning electron microscope (SEM) micrograph; b) a TEM micrograph of P3HT:PCBM (core)–PCL (sheath) fibers (2.5 μm and 200 nm scale bars, respectively); c) an SEM micrograph of P3HT:PCBM nanofibers after removal of the PCL sheath (2 μm scale bar), and; d) a high-resolution TEM micrograph of the P3HT:PCBM fibers after removal of the sheath PCL (25 nm scale bar).

The pure P3HT:PCBM fibers were incorporated into the active layers of BHJ–OPV devices by spin coating from a dispersion of fibers in cyclopentanone. Next, a homogeneous solution of P3HT:PCBM was deposited to completely backfill the porous fibrous network, forming a uniform active layer for the device (Figure 1, schematic). While this resulted in partial redissolution of the fibers, the fibers still served as a template for the soluble P3HT. This methodology has been previously reported[32] for OPV fabrication using solution-processed fibers. Device characteristics for fiber-based and thin-film devices averaged over 20 devices on at least 6 different films are presented in **Table 1**. The best-performing device from each sample is given in **Table 2**, with the corresponding current density–voltage curves shown in **Figure 2**. Each sample had a film thickness of ~100 nm. With the inclusion of electrospun P3HT:PCBM fibers to unannealed P3HT:PCBM layers, the short-circuit current density (J_{sc}) and fill factor (FF) both increased by, on average, 0.7 mA cm^{-2} and 4%, respectively, resulting in a power-conversion efficiency (PCE) increase from 1.6% to 2.0%. This represents a 25% increase from the unannealed P3HT:PCBM film devices. The highest PCE achieved for the unannealed devices was 2.3% and 2.6% for thin-film and electrospun fiber-based devices, respectively. After thermal annealing for 10 min at 160 °C, both fiber and film devices exhibited a decrease in the open-circuit voltage (V_{oc}) and increases in J_{sc}, FF, and PCE. Devices with electrospun P3HT:PCBM fibers had, on average, a 1.0 mA cm^{-2} increase in J_{sc}, a 9% increase in FF, and a 0.8% increase in PCE compared to thin film-based annealed devices.

Table 1. Average values of open-circuit voltage (V_{oc}), short-circuit current (J_{sc}), fill factor (FF), and power-conversion efficiency (η) for each device.

Sample	V_{oc} [V]	J_{sc} [mA cm^{-2}]	FF [%]	*PCE* [%]
P3HT:PCBM Film	0.67 ± 0.04	6.1 ± 0.5	40 ± 4	1.6 ± 0.3
P3HT:PCBM Film (annealed)	0.58 ± 0.02	8.7 ± 0.7	46 ± 6	2.4 ± 0.5
P3HT:PCBM Fibers	0.65 ± 0.03	6.8 ± 0.9	44 ± 6	2.0 ± 0.5
P3HT:PCBM Fibers (annealed)	0.59 ± 0.01	9.7 ± 0.6	55 + 4	3.2 ± 0.4

Table 2. Device characteristics of the best-performing devices of each sample type.

Sample	V_{oc} [V]	J_{sc} [mA cm^{-2}]	FF [%]	*PCE* [%]
P3HT:PCBM Film	0.64	6.7	46	2.3
P3HT:PCBM Film (annealed)	0.59	10.0	54	3.2
P3HT:PCBM Fibers	0.63	8.1	52	2.6
P3HT:PCBM Fibers (annealed)	0.59	10.7	63	4.0

The highest PCEs achieved for the annealed thin film- and electrospun fiber-based devices were 3.2% and 4.0%, respectively. The increases in J_{sc} and FF are indicative of increased photon absorption, increased free-charge generation, decreased charge recombination, and/or increased charge mobility.[2] No change

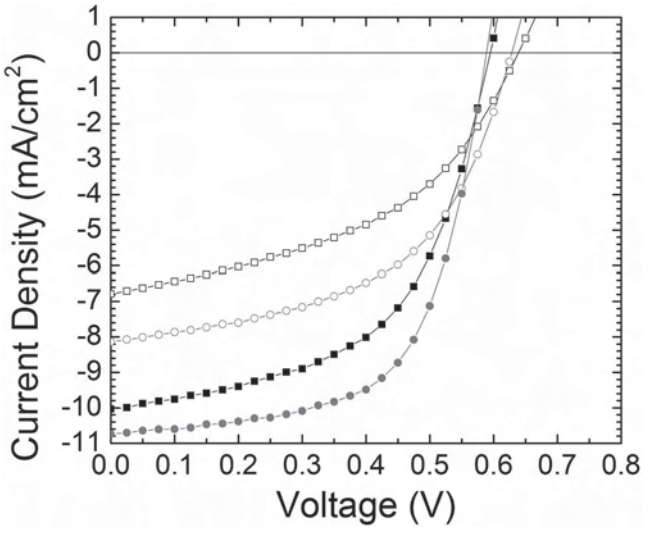

Figure 2. Current density–voltage curves for devices with active layers of P3HT:PCBM films from chlorobenzene (-□-), P3HT:PCBM films from chlorobenzene annealed at 160 °C for 10 min (-■-), P3HT:PCBM fibers with a P3HT:PCBM backfill layer (-○-), and P3HT:PCBM fibers with a P3HT:PCBM backfill layer annealed at 160 °C for 10 min (-●-) under AM1.5 conditions at 100 mW cm^{-2}. Curves are from devices described in Table 2.

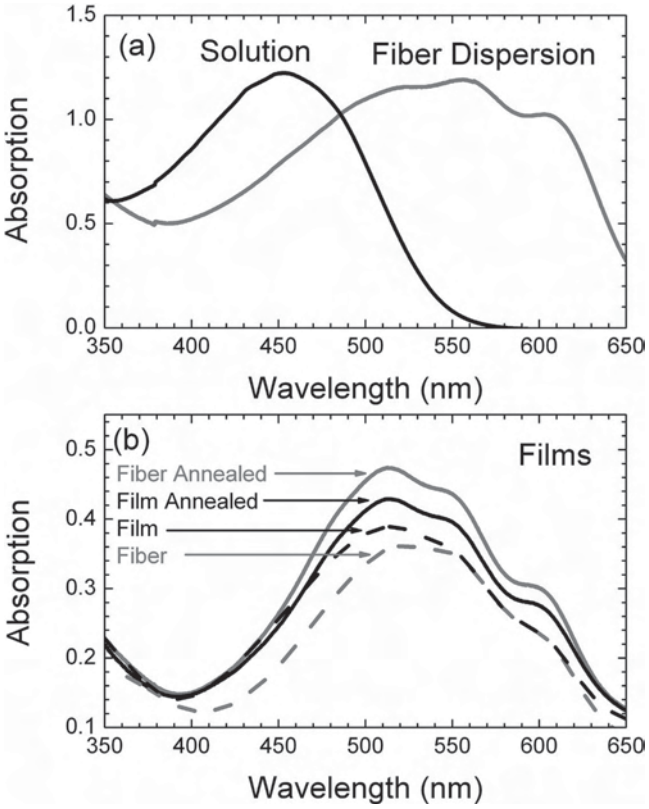

Figure 3. Visible absorption spectra of a) P3HT:PCBM solution in chlorobenzene (black line) and P3HT:PCBM fiber dispersion in cyclopentanone. b) BHJ–OPV devices: unannealed P3HT:PCBM films (black, dashed line), films annealed at 160 °C for 10 min (black, solid line), unannealed P3HT:PCBM fibers with a P3HT:PCBM backfill layer (red, dashed line), and those annealed at 160 °C for 10 min (red, solid line). All devices are ~100 nm in thickness.

in the V_{oc} was seen between fiber- and film only-based devices. Device characteristics of thin-film devices are consistent with those seen in the literature for the same P3HT:PCBM ratio and annealing procedure.[76,77]

To investigate the origin of this increased PCE in devices which incorporate electrospun fibers, the P3HT:PCBM active layers were characterized using optical absorption spectroscopy, ellipsometery, diffraction measurements, and atomic force microscopy. The visible absorption spectra for solutions, fiber dispersions in cyclopentanone, and thin-film devices of P3HT:PCBM are shown in **Figure 3**. P3HT solution in chlorobenzene shows a broad absorption with a peak at ~450 nm (Figure 3a, black line). The dispersion of electrospun fibers in cyclopentanone shows two distinct peaks at ~560 and ~610 nm with a shoulder peaks at ~520 nm (Figure 3a, red line). This redshift in absorption characteristics from the solubilized P3HT is indicative of an increase in the conjugation length of the dispersed fibers of P3HT:PCBM. These peaks correspond to a π–π* transition in solidified P3HT,[78,79] with the shoulder peak being attributed to strong interchain interactions.[80] These features are also observed in P3HT fibers made by solution processing reported by Berson et al.,[32] although the 610 nm shoulder is lower in relative magnitude compared to the solidified absorption peaks. This suggests the presence of stronger interchain interactions from the electrospun fibers. The fiber- and film-based device absorption spectra are shown in Figure 3b. The unannealed fiber device exhibits a small redshift (~10 nm) from the unannealed thin-film device, which is attributed to an increased conjugation length. The absorbance of both thin film- and fiber-based devices is increased after annealing, particularly for the electrospun fiber-based device. A second peak appears at ~550 nm, along with a shoulder peak at 610 nm, which again reflects an increase in P3HT interchain interactions. The transition dipole moment of the π–π* transition in P3HT is oriented along the polymer chain axis.[81] As light impinges onto the BHJ normal to the substrate, an increase in absorption between films of identical thicknesses would be due to the increased overlap between the transition dipole moment and the electric-field vector of the incoming light. The increased absorption in the electrospun fiber-based device is thus due to a comparatively larger percentage of polymer chains aligned parallel to the substrate. This increase in photon absorption will lead to an increase in exciton formation, which in turn will lead to a larger amount of photogenerated carriers.[82]

Electron and X-ray diffraction measurements were performed in order to study the structural order in annealed fibers and devices. For reference, two crystal planes [(100) and (020)] corresponding to the main diffraction peaks in P3HT are shown in **Figure 4**a.[83] Figure 4b shows a TEM micrograph of P3HT:PCBM fibers after removal of the PCL sheath and subsequent annealing. The corresponding electron diffraction pattern is shown in Figure 4c. The P3HT:PCBM fibers show strong diffractions from (100) and (020) planes and show a diffraction pattern exhibiting fiber symmetry. As chain alignment is often observed in electrospun fibers and both (100) and (020)

DOI: 10.1002/aenm.201100674

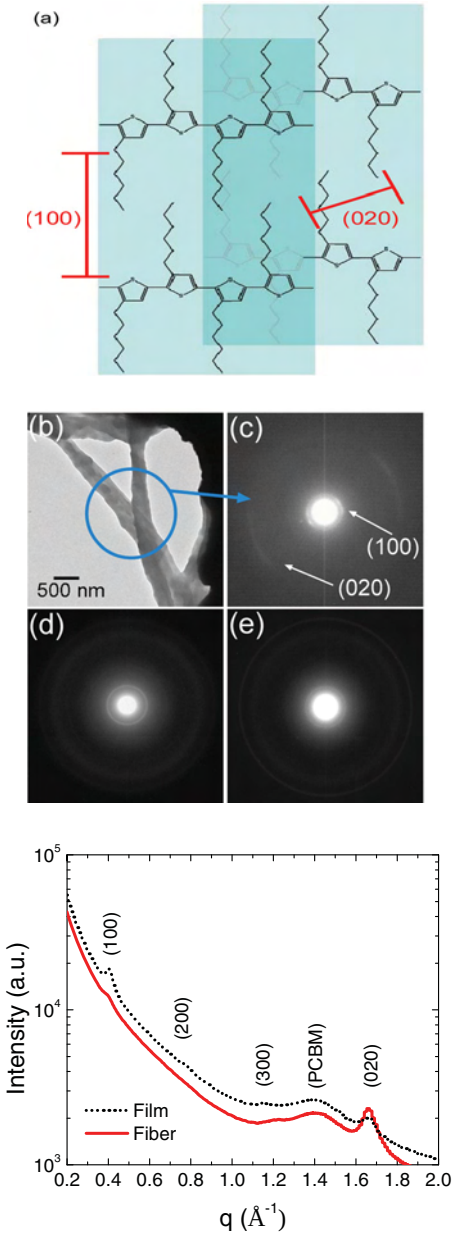

Figure 4. a) Schematic of P3HT crystal structure with (100) and (020) planes highlighted; b) TEM micrograph of pure P3HT:PCBM fibers annealed for 160 °C for 10 min; c) electron diffraction pattern of the section shown in (b) exhibiting fiber symmetry; d) electron diffraction pattern from a P3HT:PCBM film annealed for 160 °C for 10 min; e) electron diffraction pattern from a film of P3HT:PCBM fibers with a P3HT:PCBM backfill layer annealed at 160 °C for 10 min, and; f) 1D scans of (d) (dash lines) and (e) (solid lines).

diffractions are observed, it is probable that the polymer chains are aligned along the fiber axis with a mixture of [100] and [010] directions oriented radially along the fiber. For comparison, Ihn et al.[84] have shown that P3HT nanofibers made by solution-processing techniques do not exhibit the (100) reflections in electron diffraction patterns as these planes are parallel to the electron beam. Electron diffraction patterns of the annealed P3HT:PCBM films both with and without incorporated electrospun fibers are shown in Figure 4d and e, respectively. One-dimensional scans are shown in Figure 4f, in terms of the scattering vector q. The annealed P3HT:PCBM film exhibits reflections from both the (100) and (020) planes, with a more intense diffraction intensity seen from the (100) plane in this orientation (with the electron beam normal to the substrate plane). The annealed active layer derived from the electrospun fibers shows a different diffraction pattern: diffraction peaks from the (100) and (020) planes are observed, but the (020) peak is much more intense than the (100) peak. This is evidence that the two devices exhibit different preferences in P3HT crystallite orientation. Since the (020) planes show a stronger diffraction in the fiber-derived active layer and a higher optical absorption is observed, a higher quantity of P3HT molecules are likely oriented with the [100] direction normal to the substrate. Without predeposited electrospun fibers, the P3HT:PCBM film exhibits a higher intensity in (100) relative to (020). As such, a larger percentage of P3HT polymer chains are likely oriented with the [010] direction, perpendicular to the substrate, in the film device.

Glancing incidence X-ray diffraction (GIXD) results (**Figure 5**) provide complementary information that confirms the results from the electron diffraction measurements. The 2D pattern for the P3HT:PCBM film-only active layer (Figure 5a) shows a more intense (020) diffraction peak compared to the electrospun fiber-based active layer (Figure 5b). Conversely, the (100) and higher-order (200) and (300) planes are more intense in the fiber-derived active layer compared to the P3HT:PCBM film. This is more evident in the corresponding 1D patterns shown in Figure 5c. For the electrospun fiber-based active layer, the (100) set of reflections are more intense than the (020) on the meridian, which indicates that a higher percentage of P3HT crystallites have the π-stacking direction oriented parallel to the substrate. The opposite is seen for the active layer without electrospun fibers, as the (020) peak appears more intense than the (100) peak. With respect to the P3HT crystallite orientation, these results are consistent with those obtained using electron diffraction, as both of these experimental methods provide orthogonal information. As such, the intensity ratio between the (100) and (020) directions should be reversed when comparing the electron diffraction and GIXD data. Herman's orientation parameters were calculated from the azimuthal angle scans (Figure S2, Supporting Information) for both electrospun-fiber and thin-film devices. Crystallites in a sample are perfectly aligned if the orientation parameter equals one, while a completely isotropic sample has an orientation parameter of zero. The active layer with electrospun fibers exhibits a larger orientation parameter (0.72) in the (100) planes than the thin-film active layer (0.56). This indicates a better in-plane alignment of these crystallites.

The distinct orientation difference between the two samples is caused by the presence of electrospun fibers within the active layer, which ultimately leads to the difference in device performance. After the backfill deposition of solubilized P3HT:PCBM onto the electrospun P3HT:PCBM fibers, it is probable that the fibers act as a template for in-plane chain alignment throughout the active layer. This conclusion is logical when considering the increased optical absorption due to in-plane alignment of the

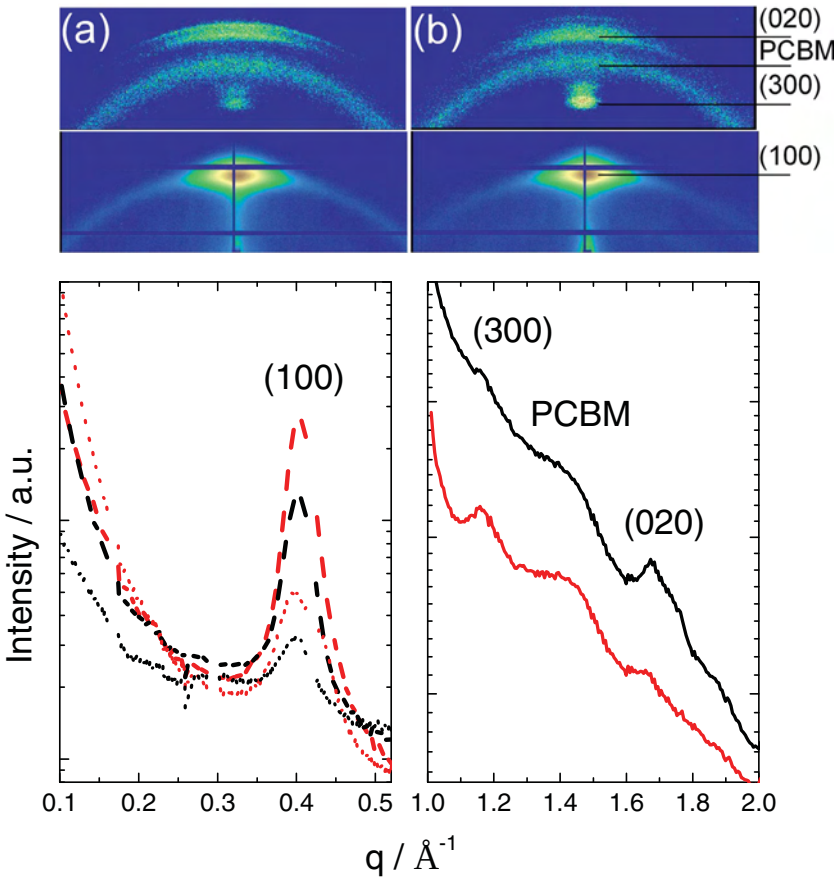

Figure 5. Two-dimensional GIXD patterns of devices consisting of a) a P3HT:PCBM active layer annealed for 160 °C for 10 min, and b) a fiber-based P3HT:PCBM active layer annealed at 160 °C for 10 min. The top pattern was generated from wide-angle scattering and the bottom from small-angle scattering. c) Corresponding small-angle (dashed lines) and wide-angle (solid lines) diffraction patterns of P3HT:PCBM films (black lines) and fiber-based P3HT:PCBM films (red lines).

π–π* transition along the polymer backbone (Figure 3b) and the fiber symmetry displayed in annealed P3HT:PCBM fibers (Figure 4c). Increased photon absorption would lead to the generation of more excitons, which in turn increases the number of carriers potentially available for collection. It is presumed that regions in the electrospun fiber-based active layer not in the vicinity of the predeposited fibers adopt a crystallite orientation similar to that of the thin-film active layer, with π-stacking predominately normal to the substrate and a comparatively lower amount of in-plane polymer chains. Charge transport is found to be highest along the polymer backbone, then through π-stacking, and finally through alkyl chains in P3HT.[85,86] The fibrous regions are thus responsible for increased photon absorption and in-plane charge transport, while the nonfibrous regions transport charge to the appropriate electrodes. The thin film-based devices comparatively lack the amount of in-plane chain alignment and thus do not absorb as many photons, leading to a lower PCE.

The surface roughness and surface morphology of the devices was studied using atomic force microscopy (AFM; **Figure 6**). The surface of a P3HT:PCBM BHJ has been shown to be rich in P3HT for films made from spin coating and thus is not representative of the bulk morphology,[87,88] leaving AFM data to be often overinterpreted. However, the inclusion of electrospun fibers (on the size scale of the BHJ thickness) likely invokes a unique morphology and surface roughness and thus should be examined. Height images from unannealed and annealed thin-film devices are shown in Figure 6a and c, respectively. The root-mean-square (RMS) surface roughness from these devices is 6.22 Å for the unannealed device and 9.06 Å for the annealed device. These values are comparable to what is typically observed for such films.[89] The addition of electrospun P3HT:PCBM fibers to the active layer yields an RMS surface roughness of 9.41 Å (Figure 6e), which is larger than the annealed device without electrospun fibers. Further annealing of the fiber-based active layer yields an RMS surface roughness double that of the unannealed device (18.4 Å, Figure 5g). While an increase in surface roughness is often thought to be a 'signature' of higher-efficiency devices,[30] it is difficult to completely decouple the effects of an altered BHJ morphology and an increased surface roughness on device performance. The nanoscale phase separation was studied using phase imaging, wherein 'hard' and 'soft' segments yielded different contrast levels in the image. The unannealed P3HT:PCBM film device shows small domains of P3HT and PCBM (Figure 6b), which, after annealing, characteristically become larger (Figure 6d).[22] Devices with the inclusion of electrospun P3HT:PCBM fibers show a very different morphology for both unannealed (Figure 6f) and annealed (Figure 6h) devices. The morphologies show anisotropic features that are much smaller (~15 nm) than the electrospun P3HT:PCBM fibers, which tend to partially orient in a similar direction over 200–500 nm length scales. It is likely that these oriented regions are remnants from the electrospun P3HT:PCBM fibers. Due to electron beam damage, the in-plane orientation of these P3HT crystallites could not be captured with TEM. However, optical absorption data (Figure 3b) suggest these anisotropic features, absent in the thin-film devices, must have P3HT chains aligned in the plane of the substrate. Furthermore, the refractive index for P3HT:PCBM films (1.77–1.80) is lower than for the P3HT:PCBM fiber-based active layers (1.91–2.01) of unannealed devices, which suggests that these anisotropic features scatter more of the incoming light. The introduction of light scattering features in BHJ–OPV devices has been previously shown to lead to increased PCEs.[90,91]

3. Conclusion

P3HT:PCBM fibers were made via coaxial electrospinning using PCL as the sacrificial sheath material. By using coaxial

Adv. Energy Mater. 2012,
DOI: 10.1002/aenm.201100674

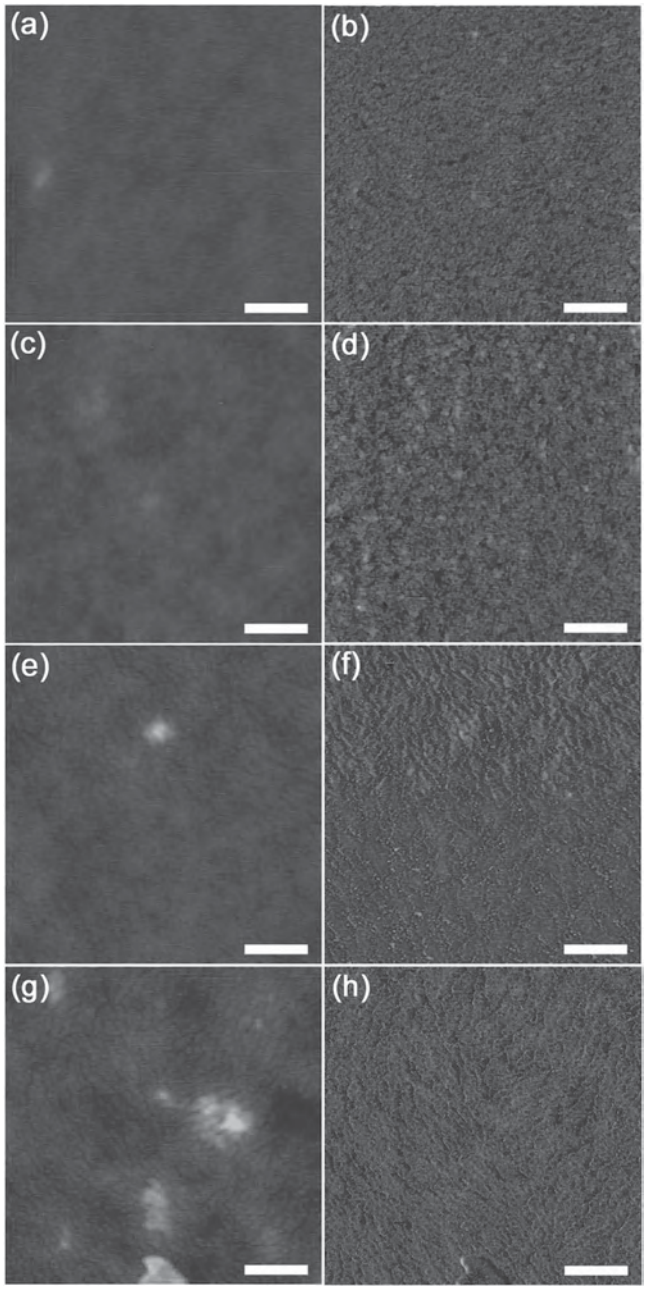

Figure 6. AFM topography (left) and phase images (right) of devices from a,b) an as-cast film of P3HT:PCBM, c,d) an annealed film of P3HT:PCBM at 160 °C for 10 min, e,f) P3HT:PCBM fibers with a P3HT:PCBM backfill layer, and g,h) P3HT:PCBM fibers with a P3HT:PCBM backfill layer annealed at 160 °C for 10 min. All height images have a 15 nm *z*-axis range. All images are 1 μm × 1 μm.

electrospinning, a uniform phase separation between the PV materials and the more easily electrospun polymer can be achieved which is not possible by simply blending the materials. Selectively stripping the PCL from the coaxial fibers yields pure P3HT:PCBM nanofibers. When embedded within the active layer, these fibers likely act as templates for increased in-plane polymer chain alignment in these devices and invoke an orientation beneficial for higher charge mobility. This altered orientation leads to increased J_{sc}, FF, and PCE values in the BHJ–OPV devices compared to films of P3HT:PCBM of identical composition. On average, the PCE increases from 2.4 to 3.2% in annealed samples, with the best devices obtaining a PCE of 3.2 and 4.0% for thin films and electrospun-based devices, respectively. The use of electrospun fibers within the active layer of BHJ–OPV is a promising methodology for improving the performance of such devices. This methodology is more practical than creating free-standing 'solar clothes' due to the ease of device fabrication and the resulting increased PCEs that are more useful for real-world PV applications. Thermal solution processing of polymeric nanofibers is only possible if the material can dissolve at an elevated temperature in a particular solvent and recrystallize in a fibrous manner once the temperature has been lowered. This likely cannot be done in the presence of another molecular moiety such as an electron-accepting material. Electrospinning allows for a relatively large amount of fibrous material of almost any composition to be easily generated in a short amount of time which can be implemented into the active layer of a device. The use of coaxial electrospinning in particular is even more advantageous as it avoids issues with blended polymer morphologies, uses smaller quantities of active-layer material, and uses an electrospinning process largely governed by the electrospinnability of the sheath material. While this initial study has focused on the use of P3HT:PCBM, it is likely that this methodology for creating electrospun fibers can be extended to other electron donor–electron acceptor material systems.

4. Experimental Section

Electrospinning: Coaxial electrospinning was performed using a concentric stainless steel nozzle (Nisco Engineering) with an outer diameter of 0.8 mm and an inner diameter of 0.35 mm. Sheath solutions of PCL (M_w = 80 kDa, Sigma) were made in 60/40 (v/v) chloroform/dimethylformamide at a concentration of 14 wt%, while core solutions of P3HT (M_w = 45 kDa, American Dye Source):PCBM (American Dye Source) were made in chloroform at 1 and 0.6 wt%, respectively. A voltage of 20 kV was applied from the coaxial nozzle to the collecting electrode using a Gamma High Voltage ES-30 power supply. The spinneret tip-to-substrate distance was set to 25 cm and flow rates for the core and sheath solutions were 1.25 and 6.5 mL h^{-1}, respectively. All electrospinning experiments were performed under ambient conditions.

Fiber Processing: Approximately 200 mg of as-electrospun core–sheath fibers were placed in 40 mL of cyclopentanone (99+%, Acros) in order to selectively dissolve the PCL component from the fibers. The resulting dispersion was centrifuged (13 000 *g*, 10 min) to pellet the P3HT:PCBM fibers and to remove the dissolved PCL. This process was repeated 6 additional times in order to fully wash the PCL from the P3HT:PCBM fibers. The fully washed fibers were redispersed in 5 mL of cyclopentanone to form a stable suspension at ~100 mg mL^{-1} for spin coating onto device substrates.

Device Fabrication: Indium tin oxide (ITO, Colorado Concept Coatings, LLC)-coated glass was selectively etched using concentrated HCl. The substrates were thoroughly cleaned with detergent, water, hexane, isopropanol, methanol, and acetone. Poly(3,4-ethylenedioxythiophene):poly(styrene sulfonate) (PEDOT:PSS, Clevios-P purchased from H. C. Starck) was filtered with a 5 μm syringe filter, deposited using spin coating, and dried at 165 °C for 20 min. When appropriate, electrospun P3HT:PCBM fibers were deposited from a cyclopentanone dispersion by spin coating. A solution of P3HT:PCBM (15:9 mg mL^{-1} in chlorobenzene) was used to interconnect the fibers and was deposited

using spin coating after filtration with a 0.45 µm syringe filter. This solution was heated to 60 °C prior to spin coating. When appropriate, the devices were annealed at 160 °C for 10 min. The resulting active layers were all ~100 nm in thickness. Aluminum electrodes were evaporated onto the substrate at a thickness of ~100 nm. The active surface area of the device was 0.16 cm^2. Spin coating of solubilized P3HT:PCBM layer, device annealing, and electrode evaporation were performed in a glove box under dry N_2.

Characterization: Current–voltage characteristics were obtained with a Keithley 237 High Voltage Source under AM1.5 solar radiation at a power density of 100 mW cm^{-2} using a Newport Oriel Full Spectrum Solar Simulator under N_2. Fiber morphologies were studied using a FEI/Phillips XL30 field-emission environmental SEM (FE-ESEM) and Philips CM-200 TEM. UV–visible absorption spectra were obtained using a Perkin Elmer Lambda 900 UV/Vis/NIR spectrometer. P3HT:PCBM surface phase separation was studied with an AFM in tapping mode using a Veeco Dimension 3100 Scanning Probe Microscope equipped with a NanoScope V controller. Electron diffraction experiments were performed using Philips CM-200 TEM. Active layers were removed from device substrates by slowly dipping the devices in water to remove the PEDOT:PSS under-layer. Fragments of the P3HT:PCBM active layers were then collected on copper TEM grids. Synchrotron experiments were carried out at the small/wide-angle X-ray scattering (SAXS/WAXS) beamline 7.3.3 of the Advanced Light Source at Lawrence Berkeley National Laboratory at 10 keV (1.24 Å) from a bend magnet and focused via a Mo/B4C double multilayer monochromator. SAXS and WAXS were carried out simultaneously using high-speed Dectris Pilatus 100k and Dectris Pilatus 1M detectors. Time-resolved experiments were performed at 10 Hz frame collection. 2D images were reduced using Nika macros for Igor Pro.[92] Images were corrected for transmission, background, and initial beam-intensity fluctuations. Refractive index measurements were performed on an Alpha-SE model ellipsometer from J.A. Woollam. Active layers were created on silicon as described above under 'Device Fabrication' and measured using 589 nm and Cody-Lorentz and/or Cauchy models.

Supporting Information

Supporting Information is available from the Wiley Online Library or from the author.

Acknowledgements

This work was supported in part by the Air Force Office of Scientific Research and Dayton Area Graduate Studies Institute. We would like to thank Dr. Alexander Hexemer and Dr. Eric Schaible for guidance, setup and data collection at beamline 7.3.3 at Advanced Light Source/Lawrence Berkley National Laboratory. The Advanced Light Source is supported by the Director, Office of Science, Office of Basic Energy Sciences, of the US Department of Energy under Contract No. DE-AC02-05CH11231.

Received: November 8, 2011
Revised: January 16, 2012
Published online:

[1] G. Dennler, M. C. Scharber, C. J. Brabec, *Adv. Mater.* **2009**, *21*, 1323–1338.
[2] J. Peet, A. J. Heeger, G. C. Bazan, *Acc. Chem. Res.* **2009**, *42*, 1700–1708.
[3] A. J. Moulé, K. Meerholz, *Adv. Funct. Mater.* **2009**, *19*, 3028–3036.
[4] B. C. Thompson, J. M. J. Fréchet, *Angew. Chem. Int. Ed.* **2008**, *47*, 58–77.
[5] C. J. Brabec, J. A. Hauch, P. Schilinsky, C. Waldauf*Mater. Res. Soc. Bull.* **2005**, *30*, 50–52.
[6] W. Ma, C. Yang, X. Gong, K. Lee, A. J. Heeger, *Adv. Funct. Mater.* **2005**, *15*, 1617–1622.
[7] G. Li, V. Shrotriya, J. Huang, Y. Yao, T. Moriarty, K. Emery, Y. Yang, *Nat. Mater.* **2005**, *4*, 864–868.
[8] M. Reyes-Reyes, K. Kim, J. Dewald, R. López-Sandoval, A. Avadhanula, S. Curran, D. L. Carroll, *Org. Lett.* **2005**, *7*, 5749–5752.
[9] H.-Y. Chen, J. Hou, S. Zhang, Y. Liang, G. Yang, Y. Yang, L. Yu, G. Li, *Nat. Photonics* **2009**, *3*, 649–653.
[10] S. H. Park, A. Roy, S. Beaupré, S. Cho, N. Coates, J. S. Moon, D. Moses, M. Leclerc, K. Lee, A. J. Heeger, *Nat. Photonics* **2009**, *3*, 297–303.
[11] Y. Lang, D. Feng, Y. Wu, S.-T. Tsai, G. Li, C. Ray, L. Yu, *J. Amer. Chem. Soc.* **2009**, *131*, 7792–7799.
[12] Y. Lang, Y. Wu, D. Feng, S.-T. Tsai, H.-J. Son, G. Li, L. Yu, *J. Amer. Chem. Soc.* **2009**, *131*, 56–57.
[13] C.-P. Chen, S.-H. Chan, T.-C. Chao, C. Ting, B.-T. Ko, *J. Amer. Chem. Soc.* **2008**, *130*, 12828–12833.
[14] N. Blouin, A. Michaud, M. Leclerc, *Adv. Mater.* **2007**, *19*, 2295–2300.
[15] J. Chen, Y. Cao, *Acc. Chem. Res.* **2009**, *42*, 1709–1718.
[16] O. Inganäs, F. Zhang, M. R. Andersson, *Acc. Chem. Res.* **2009**, *42*, 1731–1739.
[17] J. Y. Kim, K. Lee, N. E. Coates, D. Moses, T.-Q. Nguyen, M. Dante, A. J. Heeger, *Science* **2007**, *317*, 222–225.
[18] A. Hadipour, B. de Boer, P. W. M. Blom, *J. Appl. Phys.* **2007**, *102*, 074506.
[19] S. Sista, M.-H. Park, Z. Hong, Y. Wu, J. Hou, W. K. Kwan, G. Li, Y. Yang, *Adv. Mater.* **2010**, *22*, 380–383.
[20] T. Ameri, G. Dennler, C. Lungenschmied, C. J. Brabec, *Energy Environ. Sci.* **2009**, *2*, 347–363.
[21] T. M. Clarke, A. M. Ballantyne, J. Nelson, D. D. C. Bradley, J. R. Durrant, *Adv. Funct. Mater.* **2008**, *18*, 4029–4035.
[22] A. L. Ayzner, D. D. Wanger, C. J. Tassone, S. H. Tolbert, B. J. Schwartz, *J. Phys. Chem. C* **2008**, *122*, 18711–18716.
[23] M. Al-Ibrahim, O. Ambacher, S. Sensfuss, G. Gobsch, *Appl. Phys. Lett.* **2005**, *86*, 201120.
[24] G. Li, Y. Yao, H. Yang, V. Shrotriya, G. Yang, Y. Yang, *Adv. Funct. Mater.* **2007**, *17*, 1636–1644.
[25] H. Tang, G. Lu, L. Li, J. Li, Y. Wang, X. Yang, *J. Mater. Chem.* **2010**, *20*, 683–688.
[26] J. H. Park, J. S. Kim, J. H. Lee, W. H. Lee, K. Cho, *J. Phys. Chem. C* **2009**, *113*, 17579–17584.
[27] F. Zhang, K. G. Jespersen, C. Björström, M. Svensson, M. R. Andersson, V. Sundström, K. Magnusson, E. Moons, A. Yartsev, O. Inganäs, *Adv. Funct. Mater.* **2006**, *16*, 667–674.
[28] J. Peet, J. Y. Kim, N. E. Coates, W. L. Ma, D. Moses, A. J. Heeger, G. C. Bazan, *Nat. Mater.* **2007**, *6*, 497–500.
[29] J. K. Lee, W. L. Ma, C. J. Brabec, J. Yuen, J. S. Moon, J. Y. Kim, K. Lee, G. C. Bazan, A. J. Heeger, *J. Amer. Chem. Soc.* **2008**, *130*, 3619–3623.
[30] Y. Yao, J. Hou, Z. Xu, G. Li, Y. Yang, *Adv. Funct. Mater.* **2008**, *18*, 1783–1789.
[31] A. J. Moulé, K. Meerholz, *Adv. Mater.* **2008**, *20*, 240–245.
[32] S. Berson, R. De Bettignies, S. Bailly, S. Guillerez, *Adv. Funct. Mater.* **2007**, *17*, 1377–1384.
[33] Y. Zhao, S. Shao, Z. Xie, Y. Geng, L. Wang, *J. Phys. Chem. C* **2009**, *113*, 17235–17239.
[34] H. Xin, F. S. Kim, S. A. Jenekhe, *J. Amer. Chem. Soc.* **2008**, *130*, 5424–5425.
[35] H. Xin, G. Ren, F. S. Kim, S. A. Jenekhe, *Chem. Mater.* **2008**, *20*, 6199–6207.
[36] D. Li, Y. Xia, *Adv. Mater.* **2004**, *16*, 1151–1170.

[37] S. Agarwal, A. Greiner, J. H. Wendorff, *Adv. Funct. Mater.* **2009**, *19*, 2863–2879.
[38] D. H. Reneker, I. Chun, *Nanotechnol.* **1996**, *7*, 216–223.
[39] D. Lukas, A. Sarkar, P. Pokomy, *J. Appl. Phys.* **2008**, *103*, 084309.
[40] A. Kumar, M. Wei, C. Barry, J. Chen, J. Mead, *Macromol. Mater. Eng.* **2010**, *295*, 701–708.
[41] G. Kim, Y.-S. Cho, W. D. Kim, *Eur. Polym. J.* **2006**, *42*, 2031–2038.
[42] E. Kostakova, L. Meszaros, J. Gregr, *Mater. Lett.* **2009**, *63*, 2419–2422.
[43] M. Zukalova, J. Prochazka, Z. Bastl, J. Duchoslav, L. Rubacek, D. Havlicek, L. Kavan, *Chem. Mater.* **2010**, *22*, 4045–4055.
[44] J. Xie, X. Li, Y. Xia, *Macromol. Rapid Comm.* **2008**, *29*, 1775–1792.
[45] H. S. Yoo, T. G. Kim, T. G. Park, *Adv. Drug Del. Rev.* **2009**, *61*, 1033–1042.
[46] Y. Ner, J. G. Grote, J. A. Stuart, G. A. Sotzing, *Angew. Chim. Int. Ed.* **2009**, *48*, 5134–5138.
[47] G. Kwak, G. H. Lee, S.-H. Shim, K.-B. Yoon, *Macromol. Rapid Commun.* **2008**, *29*, 815–820.
[48] E. Formo, E. Lee, D. Campbell, Y. Xia, *Nano Lett.* **2008**, *8*, 668–672.
[49] S. Zhan, D. Chen, X. Jiao, C. Tao, *J. Phys. Chem. B* **2006**, *110*, 11199–11204.
[50] H.-W. Lu, L. Yu, W. Zheng, Y.-S. Li, Z.-W. Fu, *Electrochem. Solid-State Lett.* **2008**, *11*, A140–A144.
[51] L. Ji, X. Zhang, *Nanotechnol.* **2009**, *20*, 155705.
[52] C. Chang, V. H. Tran, J. Wang, Y.-K. Fuh, L. Lin, *Nano Lett.* **2010**, *10*, 726–731.
[53] A. R. S. Priya, A. Subramania, Y.-S. Jung, K.-J. Kim, *Langmuir* **2008**, *24*, 9816–9819.
[54] X.-S. Qin, S.-Y. Wang, *J. Appl. Polym. Sci.* **2006**, *102*, 1285–1290.
[55] P. Heikkilä, A. Taipale, M. Lehtimäki, A. Harlin, *Polym. Engin. Sci.* **2008**, *48*, 1168–1176.
[56] M. Wang, N. Jing, C. B. Su, J. Kameoka, C.-K. Chou, M.-C. Hung, K.-A. Chang, *Appl. Phys. Lett.* **2006**, *88*, 033106.
[57] N. M. Bedford, A. J. Steckl, *ACS Appl. Mater. Interfaces.* **2010**, *2*, 2448–2455.
[58] H. Liu, C. H. Reccius, H. G. Craighead, *Appl. Phys. Lett.* **2005**, *87*, 253106.
[59] S. Lee, G. D. Moon, U. Jeong, *J. Mater. Chem.* **2009**, *19*, 743–748.
[60] S. W. Lee, H. J. Lee, J. H. Choi, W. G. Koh, J. M. Myoung, J. H. Hur, J. J. Park, J. H. Cho, U. Jeong, *Nano Lett.* **2010**, *10*, 347–351.
[61] C.-C. Kuo, C.-T. Wang, W.-C. Chen, *Macromol. Symp.* **2009**, *279*, 41–47.
[62] A. Laforgue, L. Robitaille, *Synth. Met.* **2008**, *158*, 577–584.
[63] S. Chuangchote, M. Fujita, T. Sagawa, H. Sakaguchi, S. Yoshikawa, *ACS Appl. Mater. Interfaces* **2010**, *2*, 2995–2997.
[64] N. D. Treat, M. A. Brady, G. Smith, M. F. Toney, E. J. Kramer, C. J. Hawker, M. L. Chabinyc, *Adv. Energy Mater.* **2011**, *1*, 82–89.
[65] B. Schmidt-Hansberg, M. Sanyal, M. F. G. Klein, M. Pfaff, N. Schnabel, S. Jaiser, A. Vorobiev, E. Müller, A. Colsmann, P. Scharfer, D. Gerthsen, U. Lemmer, E. Barrena, W. Schabel, *ACS Nano* **2011**, *5*, 8579–8590.
[66] S. Sundarrajan, R. Murugan, A. S. Nair, S. Ramakrishna, *Mater. Lett.* **2010**, *64*, 2369–2372.
[67] S. O. Han, J. H. Youk, K. D. Min, Y. O. Kang, W. H. Park, *Mater. Lett.* **2008**, *62*, 759–762.
[68] J. M. Deitzel, J. Kleinmeyer, D. Harris, N. C. B. Tan, *Polymer* **2001**, *42*, 261–272.
[69] S. R. Bhattarai, N. Bhattarai, H. K. Yi, P. H. Hwang, D. I. Cha, H. Y. Kim, *Biomaterials* **2004**, *25*, 2595–2602.
[70] H. Liu, J. Kameoka, D. A. Czaplewski, H. G. Craighead, *Nano Lett.* **2008**, *4*, 671–675.
[71] K. Zhang, X. Wang, Y. Yang, L. Wang, M. Zhu, B. S. Hsiao, B. Chu, *J. Polym. Sci., Part B: Polym. Phys.* **2010**, *48*, 1118–1125.
[72] Z. Chen, M. D. Foster, W. Zhou, H. Fong, D. H. Reneker, R. Resendes, I. Manners, *Macromolecules* **2001**, *34*, 6156–6158.
[73] P. E. Shaw, A. Ruseckas, I. D. W. Samuel, *Adv. Mater.* **2008**, *20*, 3516–3520.
[74] G. Li, V. Shrotriya, Y. Yao, Y. Yang, *J. Appl. Phys.* **2005**, *98*, 043704.
[75] A. K. Moghe, B. S. Gupta, *Polym. Rev.* **2008**, *48*, 353–377.
[76] D. H. Wang, H. K. Lee, D.-G. Choi, J. H. Park, O. O. Park, *App. Phys. Lett.* **2009**, *95*, 043505.
[77] J. Nakamura, K. Murata, K. Takahashi, *Appl. Phys. Lett.* **2005**, *87*, 132105.
[78] P. D. Cunningham, L. M. Hayden, *J. Phys. Chem. C* **2008**, *112*, 7928–7935.
[79] V. Shrotriya, J. Ouyang, R. J. Tseng, G. Li, Y. Yang, *Chem. Phys. Lett.* **2005**, *411*, 138–143.
[80] P. J. Brown, D. S. Thomas, A. Köhler, J. S. Wilson, J.-S. Kim, C. M. Ramsdale, H. Sirringhaus, R. H. Friend, *Phys. Rev. B* **2003**, *67*, 064203.
[81] M. C. Gurau, D. M. Delongchamp, B. M. Vogel, E. K. Lin, D. A. Fischer, S. Sambasivan, Lee. J. Richter, *Langmuir* **2007**, *23*, 834–842.
[82] Y. Kim, S. Cook, S. M. Tuladhar, S. A. Choulis, J. Nelson, J. R. Durrant, D. D. C. Bradley, M. Giles, I. McCulloch, C.-S. Ha, M. Ree, *Nat. Mater.* **2006**, *5*, 197–203.
[83] L. F. Drummy, R. J. Davis, D. L. Moore, M. Durstock, R. A. Vaia, J. W. P. Hsu, *Chem. Mater.* **2011**, *23*, 907–912.
[84] K. J. Ihn, J. Moulton, P. Smith, *J. Polym. Sci. Part B Polym. Phys.* **1993**, *31*, 735–742.
[85] B. O'Connor, R. J. Kline, B. R. Conrad, L. J. Richter, D. Gundlach, M. F. Toney, D. M. DeLongchamp, *Adv. Funct. Mater.* **2011**, *21*, 3697–3705.
[86] Y.-K. Lan, C.-I. Huang, *J. Phys. Chem. B* **2009**, *113*, 14555–14564.
[87] D. Chen, A. Nakahara, D. Wei, D. Nordlund, T. P. Russel, *Nano Lett.* **2011**, *11*, 561–567.
[88] A. J. Parnell, A. D. F. Dunbar, A. J. Pearson, P. A. Staniec, A. J. C. Dennison, H. Hamamatsu, M. W. A. Skoda, D. G. Lidzey, R. A. L. Jones, *Adv. Mater.* **2010**, *22*, 2444–2447.
[89] B. Xue, B. Vaughan, C.-H. Poh, K. B. Burke, L. Thomsen, A. Stapleton, X. Zhou, G. W. Bryant, W. Belcher, P. C. Dastoor, *J. Phys. Chem. C* **2010**, *114*, 15797–15805.
[90] H. K. Yu, W. J. Dong, G. H. Jung, J.-L. Lee, *ACS Nano* **2011**, *5*, 8026–8032.
[91] H. A. Atwater, A. Polman, *Nat. Mater.* **2010**, *9*, 205–213.
[92] Comprehensive data reduction macro package for converting 2D SAS area detector to 1D SAS lineout, developed by Jan Ilavsky at Argonne National Laboratory, version 1.17.

ADVANCED ENERGY MATERIALS

Supporting Information

for *Adv. Energy Mater.*, DOI: 10.1002/aenm. 201100674

Nanofiber-Based Bulk-Heterojunction Organic Solar Cells Using Coaxial Electrospinning

*Nicholas M. Bedford , Matthew B. Dickerson , Lawrence F. Drummy , Hilmar Koerner , Kristi M. Singh , Milana C. Vasudev , Michael F. Durstock , Rajesh R. Naik , * and Andrew J. Steckl **

(Supporting Information)

Fig S1. P3HT-PCBM structures obtained by electrospinning blends of (a) 3 wt% P3HT, 2.4 wt% PCBM, 1 wt% PEO in $CHCl_3$ at 0.6 kV/cm (10 μm scale bar) and (b) 13.5 wt% PCL, 2 wt% P3HT, 1.2 wt% PCBM in $CHCl_3$ at 0.6 kV/cm (5 μm scale bar) followed by subsequent removal of the insulating polymer with acetonitrile or cyclopentanone respectively.

Fig S2. Azimuthal angle of the (100), (300), and (020) reflections for P3HT:PCBM films (black lines) and fiber-based P3HT:PCBM films (red lines).

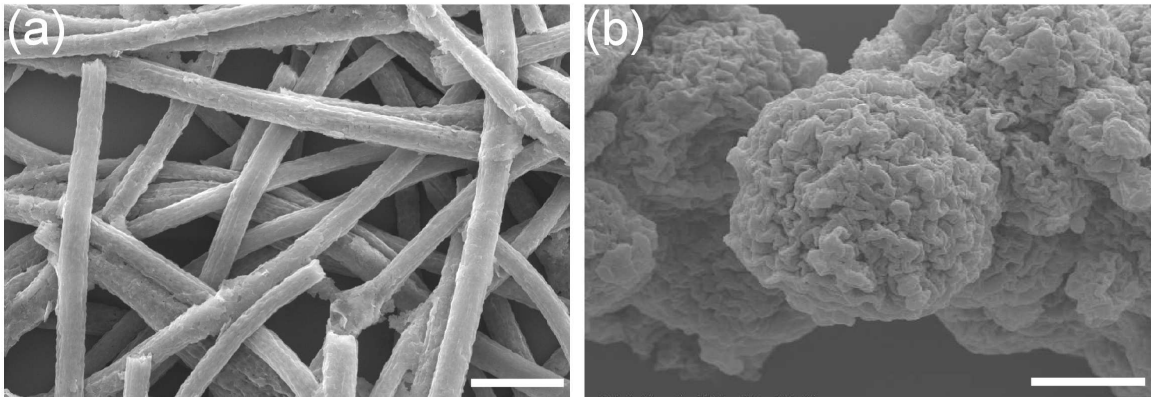

Fig. S1P3HT-PCBM structures obtained by electrospinning blends of (a) 3 wt% P3HT, 2.4 wt% PCBM, 1 wt% PEO in $CHCl_3$ at 0.6 kV/cm (10 μm scale bar) and (b) 13.5 wt% PCL, 2 wt% P3HT, 1.2 wt% PCBM in $CHCl_3$ at 0.6 kV/cm (5 μm scale bar) followed by subsequent removal of the insulating polymer with acetonitrile or cyclopentanone respectively.

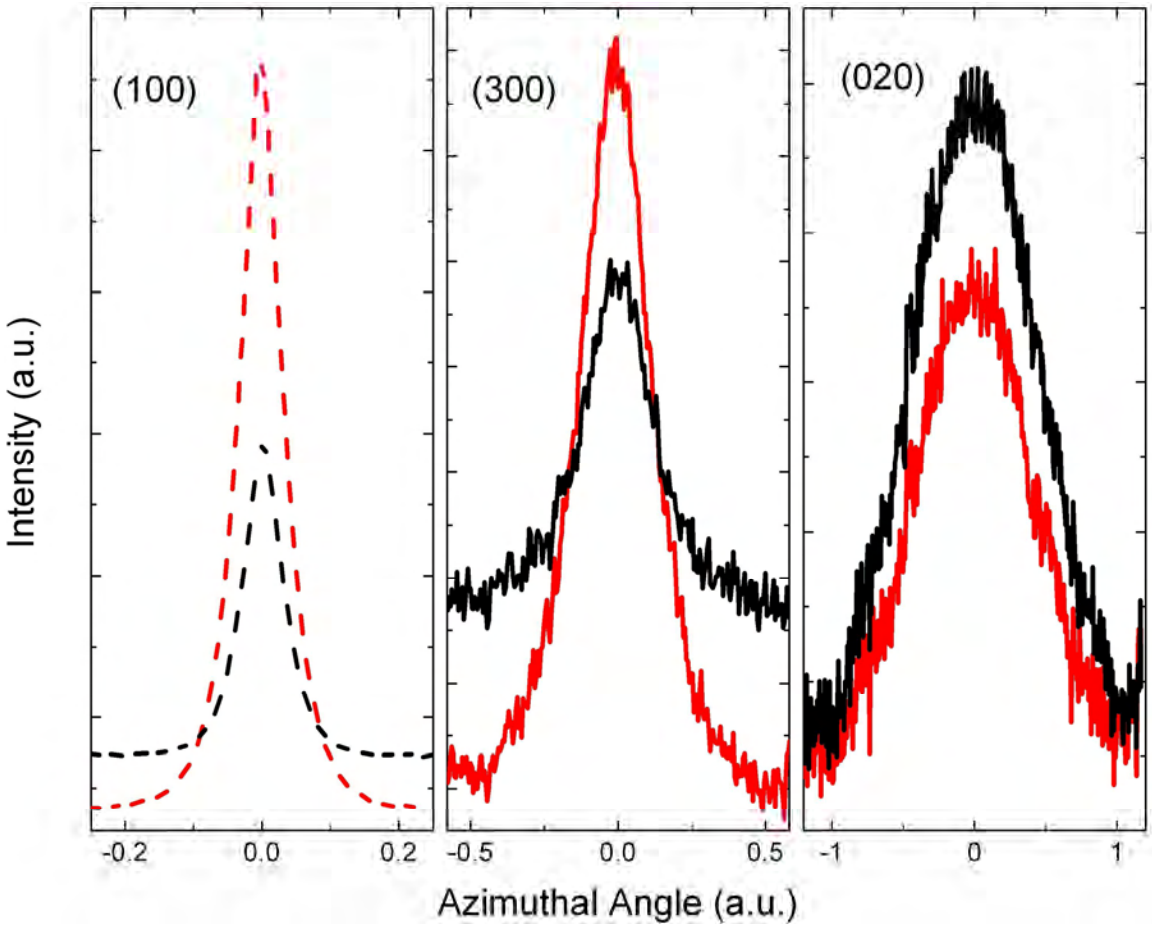

Fig. S2 Azimuthal angle of the (100), (300), and (020) reflections for P3HT:PCBM films (black lines) and fiber-based P3HT:PCBM films (red lines).